Design of Piezoelectric Energy Harvesting Systems: A Topology Optimization Approach Based on Multilayer Plates and Shells

CORY J. RUPP,[1] ANTON EVGRAFOV,[2] KURT MAUTE[3] AND MARTIN L. DUNN[1,*]

[1]*Department of Mechanical Engineering, University of Colorado, Boulder, Colorado 80309, USA*

[2]*Department of Mathematics, Technical University of Denmark, 2800 Kgs. Lyngby, Denmark*

[3]*Department of Aerospace Engineering Sciences, University of Colorado, Boulder, Colorado 80309, USA*

ABSTRACT: We develop a computational approach to analyze and design piezoelectric energy harvesting systems composed of layered plates and shells connected to an electrical circuit. The finite element method is used to model the coupled electromechanics of the piezoelectric harvesting structure and a lumped parameter model for the dynamics of the electrical circuit. We assume the harvester is subjected to a prescribed harmonic base excitation and that the structural and electrical responses are linear. We use topology optimization to design the layout of a multilayer structure consisting of structural, piezoelectric, and electrode layers, as well as the electrical circuit. The flexibility of our formalism admits the definition of specific system-level objectives, e.g., maximize the power harvested, in an algebraic fashion. After describing our analysis and design approaches, we present examples that demonstrate the versatility of our approach and show how it can be used to explore general behavior and develop overarching design principles for piezoelectric energy harvesting devices. For the objective of maximizing the power harvested, we investigate: (i) optimal designs for various piezoelectric to substrate thickness ratios, (ii) the effect of mass loading on optimal design, and (iii) the sensitivity of designs to shape variations.

Key Words: energy harvesting, optimization, piezoelectric.

INTRODUCTION

THE use of piezoelectric materials incorporated into structures to harvest energy from ambient vibrations has received significant attention over the last decade with the overarching goal of eliminating or reducing the need of external power sources or batteries to power remotely operated devices. The interest in vibrational energy harvesting has been motivated by advances in low-power electronic components such as wireless sensors and actuators, as well as advances in technologies that make it possible to fabricate such devices at ever smaller sizes. Additional motivation is provided by the desire to develop increasingly sophisticated multifunctional materials, e.g., materials that simultaneously provide structural and power functionality. As one of three methods used to convert mechanical vibrational energy to electrical energy, piezoelectric transduction, in contrast to electromagnetic and electrostatic transduction (Williams and Yates, 1996), is a viable means to achieve this goal because it can be directly incorporated into, or even replace structural components. The interest in piezoelectric energy harvesting is reflected in a number of authoritative reviews that have been written in recent years (Sodano and Inman, 2004; duToit et al., 2005; Beeby et al., 2006; Anton and Sodano, 2007; Priya, 2007; Cook-Chennault et al., 2008; Erturk and Inman, 2008a); extensive details regarding applications, experimental techniques, and modeling and design approaches can be found within these references.

Many piezoelectric energy harvester configurations consist of a flat cantilever beam covered with piezoelectric patches on one or both sides. This harvester is connected to a vibrating structure, usually at its base, in such a manner that the vibrational signature and energy of the structure is transferred to the piezoelectric energy harvester. Flat beam and plate structures are typically used for these problems because they allow for a large generation area (the larger the area, the larger the charge production) that can be actively strained by the vibration of the structure, ease of analysis, and ability to be 'tuned' to the host structure vibration signature. Generally, the vibrational input to the harvester is broadband, although most harvesting strategies have focused on a single

*Author to whom correspondence should be addresed.
E-mail: Martin.Dunn@Colorado.EDU
Figures 2–17 appear in color online: http://jim.sagepub.com

1045-389X/09/16 1923–17 $10.00/0 DOI: 10.1177/1045389X09341200

resonant frequency of the harvester, where vibrational energy is the greatest. The description of the entire energy harvesting process requires an understanding of (i) the mechanical vibrations of the structure, the (ii) electromechanics of the piezoelectric transduction, and (iii) the dynamic behavior of the electrical circuit, which are all three coupled. The first is well-known, while the incorporation of the second and third are the heart of the energy harvesting research community. Many models of varying complexity, including lumped-parameter idealizations, analytical approaches based on beam theory, and numerical approaches using the Rayleigh-Ritz or finite element method have been developed; the state-of-the-art of which is reviewed by Erturk and Inman (2008a). Less effort appears to have been focused on the circuit analysis and design specifically for piezoelectric energy harvesting. A number of authors (Ottman et al., 2002; Ottman et al., 2003; Lesieutre et al., 2004; Lefeuvre et al., 2005a, 2007; Shu and Lien, 2006a, b; Shu et al., 2007) provide sophisticated circuit designs for charging a battery with a piezoelectric energy harvester; Lefeuvre et al. (2005b) provide a comparison of some of these approaches.

Most piezoelectric energy harvesting approaches to date focus on the electromechanics of the piezoelectric transduction and use a transient or steady-state vibrational signature, usually at resonance, as input for the base excitation of the piezoelectric harvesting structure which is often coupled one-way to a simple external harvesting circuit. However, important aspects of this problem are often neglected. Erturk and Inman (2008b) and Erturk et al. (2009) demonstrate that while traditional lumped parameter analysis approaches provide much of the basic understanding, they lack important information about the coupled electromechanics, e.g., the existence of strain nodes at different resonances or the feedback of the circuit dynamics to the structural response. In their investigations of strain nodes (where the surface strain changes sign), they find that if an electrode crosses the strain node then charge cancellation occurs, degrading the performance of the piezoelectric harvester. This finding is also reported by Kim et al. (2005a, b) for circular plates which they rectify by changing the piezoelectric polarization to match the strain state and allow energy to be harvested from both tensile and compressive strain regions without cancellation. On the circuit side, complex rectifying and converting circuits have been created and optimized (Lefeuvre et al., 2005a, 2007), and in some cases include fully coupled feedback (Lesieutre et al., 2004; Elvin and Elvin, 2009), but for simplification purposes are modeled with a single or multiple degree-of-freedom lumped electromechanical model at resonance. While their techniques properly model the circuit dynamics and circuit feedback, they oversimplify the mechanical model. A proper representation of the mechanical response is necessary for optimizing the power of harvesting systems.

The use of optimization techniques to design the material layouts of piezoelectric systems for actuation or resonator systems has been studied previously. For example, Donoso and Bellido (2009) use topology optimization to find the polarization layout for piezoelectric plate actuators and sensors, while Abdalla et al. (2005) optimize the layout of a compliant mechanism to maximize the efficiency of load transfer from a piezoelectric stack actuator. Other piezoelectric actuator design methodologies using topology optimization have been reported by Carbonari et al. (2007a,b), and Drenckhan et al. (2008). Donoso and Sigmund (2009) use shape optimization to find thickness and width profiles of piezoelectric layers on a cantilever bimorph to minimize tip deflections both statically and dynamically. Ha and Cho (2006) maximize the piezoelectric coupling strength by finding optimal material layouts for piezoelectric resonators, and Kang and Tong (2008a, b) use topology optimization to find the layout of structural and piezoelectric layers, as well as the electric actuation voltages, to control the displacement field of piezoelectric plates. Zheng et al. (2009) use topology optimization to maximize mechanical to electrical energy conversion in a static sense for piezoelectric plates, and Elka and Bucher (2009) optimally distribute electrodes to tailor electromechanical modal filtering. Frecker (2003) provides a review of some of the earlier uses of optimization with piezoelectric actuators and structures.

In this article we develop a general methodology to analyze and design piezoelectric energy harvesting systems based on multilayer plate and shell structures with piezoelectric layers coupled to an external harvesting circuit. Although our approach admits shells, we will refer to the structures as plates in the following, even if they are curved. We assume that both the structural and electrical responses of the harvester and circuit are linear and excited by a harmonic base motion, allowing for time-harmonic analysis of the harvesting system. We use the finite element method to model the fully coupled components of the piezoelectric harvesting structure, namely the structural dynamics, electromechanics, and electrode conduction, while a lumped parameter approach is used to model the circuit dynamics (Figure 1). Here we model the feedback of the circuit to the piezoelectric structure as well as the response of the circuit. We use a piezoelectric layered plate formulation similar to that described by Marinkovic et al. (2007), and extend this approach for design optimization. After describing our modeling approach, we present a methodology to optimally design piezoelectric energy harvesting systems following a topology optimization approach. Topology optimization is a computational technique used to determine the layout, or topology, of a structure or material such that a prescribed objective is maximized or minimized subject to design constraints. Our approach facilitates the design of piezoelectric energy harvesters by tailoring the layout,

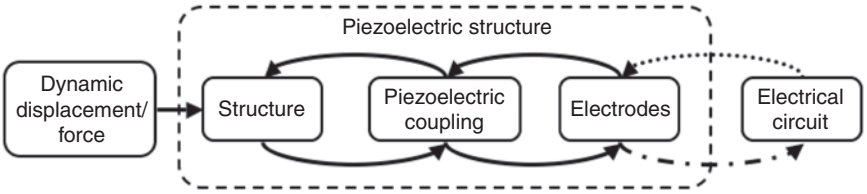

Figure 1. *Components of a piezoelectric harvesting structure as well as their coupling, including the coupling to (dash-dot line) and feedback from (dotted line) the circuit.*

both in the plane and through the thickness, of multilayer structures consisting of structural layers, piezoelectric layers, electrodes, and electrical circuit parameters. Objectives can be formulated in a flexible algebraic manner, and include for example, open circuit voltage and power output/dissipation. To the best of our knowledge, our work is the first methodology for the optimal design of piezoelectric harvesting systems by using topology optimization to design both the layout of piezoelectric and structural materials on layered plate structures as well as the harvesting circuit to which it is connected.

This paper is organized as follows: the following section details the mechanical, piezoelectric, electrode, and circuit models and their formulation in the finite element method/lumped parameter approach, including how the various fields are coupled. After a description of our analysis and design approaches, we validate our modeling approach by comparison to experiments in the literature for both beam and plate structures. Finally, we demonstrate the versatility of our approach and explore the behavior of piezoelectric energy harvesting systems with numerical examples.

ANALYSIS AND DESIGN FORMULATIONS

Field Equations

Our piezoelectric energy-harvesting model can be separated into three sub-models: the mechanics and coupled electromechanics of the piezoelectric structure, electrical conduction in the electrode, and the electrical circuit model. These sub-models are then coupled through their individual electrical interface conditions. The electrodes are explicitly modeled so that electrical connectivity is maintained between desired parts of the model (e.g., the piezoelectric material and circuit), especially as the model changes during the topology optimization procedure. In the piezoelectric mechanical/electrical model, the mechanical and electric field equations of the layered plate piezoelectric structure are written as:

$$\nabla \cdot \mathbf{T} = \rho \ddot{\mathbf{u}} \tag{1}$$

$$\nabla \cdot \mathbf{D} = 0 \tag{2}$$

where $\mathbf{T}$ is the stress tensor, ρ is the mass density, $\mathbf{u}$ is the displacement vector, and $\mathbf{D}$ is the electrical displacement vector. The mechanical and electrical fields are coupled through the piezoelectric constitutive law:

$$\begin{aligned} \mathbf{T} &= \mathbf{c}^E\mathbf{S} - \mathbf{e}\mathbf{E} \\ \mathbf{D} &= \mathbf{e}^T\mathbf{S} + \boldsymbol{\varepsilon}^S\mathbf{E} \end{aligned} \tag{3}$$

where $\mathbf{c}^E$ is the stiffness tensor at constant electric field, $\mathbf{S}$ is the strain tensor, $\mathbf{e}$ is the piezoelectric coupling tensor, $\boldsymbol{\varepsilon}^S$ is the dielectric tensor at constant strain, and $\mathbf{E}$ is the electric field vector. Following Kirchhoff plate theory where the out-of-plane normal (3-direction), shear, and inter-layer stresses are neglected ($T_{33} = 0, S_{32} = S_{31} = 0$), and by neglecting the in-plane electric fields ($E_1 = E_2 = 0$) the constitutive law can be reduced. Similar to Marinkovic et al. (2007), the constitutive equation for the i-th layer can be written as:

$$\begin{aligned} \begin{Bmatrix} \mathbf{T}'^{(i)} \\ \mathbf{D}'^{(i)} \end{Bmatrix} &= \begin{Bmatrix} T_{11}^{(i)} \\ T_{22}^{(i)} \\ T_{12}^{(i)} \\ D_3^{(i)} \end{Bmatrix} = \begin{bmatrix} Q_{11}^{(i)} & Q_{12}^{(i)} & 0 & e'^{(i)}_{31} \\ Q_{12}^{(i)} & Q_{11}^{(i)} & 0 & e'^{(i)}_{31} \\ 0 & 0 & Q_{66} & 0 \\ e'^{(i)}_{31} & e'^{(i)}_{31} & 0 & -\varepsilon'^{(i)}_{33} \end{bmatrix} \begin{Bmatrix} S_{11}^{(i)} \\ S_{22}^{(i)} \\ S_{12}^{(i)} \\ -E_3^{(i)} \end{Bmatrix} \\ &= \begin{bmatrix} \mathbf{Q}^{(i)} & \mathbf{e}'^{(i)} \\ \left(\mathbf{e}'^{(i)}\right)^T & \boldsymbol{\varepsilon}'^{(i)} \end{bmatrix} \begin{Bmatrix} \mathbf{S}'^{(i)} \\ -\mathbf{E}'^{(i)} \end{Bmatrix} \end{aligned} \tag{4}$$

where the primed notation $(\cdot)'$ indicates the coefficients are reduced, which are written as:

$$\begin{aligned} Q_{11}^{(i)} &= c_{11}^{E(i)} - \frac{\left(c_{13}^{E(i)}\right)^2}{c_{33}^{E(i)}}, \quad Q_{12}^{(i)} = c_{12}^{E(i)} - \frac{\left(c_{13}^{E(i)}\right)^2}{c_{33}^{E(i)}}, \\ Q_{66}^{(i)} &= \frac{1}{2}\left(c_{11}^{E(i)} - c_{12}^{E(i)}\right) \\ e'^{(i)}_{31} &= e_{31}^{(i)} - \frac{c_{13}^{E(i)}}{c_{33}^{E(i)}} e_{33}^{(i)}, \quad \varepsilon'^{(i)}_{33} = \varepsilon_{33}^{S(i)} + \frac{\left(e_{33}^{(i)}\right)^2}{c_{33}^{E(i)}}. \end{aligned} \tag{5}$$

Using Kirchhoff kinematics, we assume that the strains through the total thickness can be written as the sum of the midplane strains $\mathbf{S}'_0$ and the product of the curvatures $\boldsymbol{\kappa}$ with the distance from the midplane z_c (i.e., $\mathbf{S}' = \mathbf{S}'_0 + z_c\boldsymbol{\kappa}$). We also assume a constant electric

field and linear potential $\phi^{(i)}$ through the thickness of each layer (i.e., $\mathbf{E}'^{(i)} = E_3^{(i)} = -\frac{\mathrm{d}}{\mathrm{d}z}\phi^{(i)}$). Applying Hamilton's principle for the layered system of piezoelectric equations results in:

$$\int_S \sum_i^n \int_{h_-^{(i)}}^{h_+^{(i)}} (\mathbf{S}')^T \left(\mathbf{Q}^{(i)}\mathbf{S}' - \mathbf{e}'^{(i)}\mathbf{E}'^{(i)}\right) + \mathbf{u}^T\rho^{(i)}\mathbf{u} + \left(\mathbf{E}'^{(i)}\right)^T \left(\mathbf{e}'^{(i)}\mathbf{S}' + \mathbf{e}'^{(i)}\mathbf{E}'^{(i)}\right)\mathrm{d}z\mathrm{d}S = \int_S \mathbf{u}^T\hat{\mathbf{t}} - \left(\phi^{(i)}\right)^T\overline{q}^{(i)}\mathrm{d}S \tag{6}$$

where the Neumann boundary conditions are:

$$\begin{aligned} \hat{\mathbf{t}} &= \mathbf{T}\cdot\hat{\mathbf{n}} \\ \overline{q}^{(i)} &= -\mathbf{D}^{(i)}\cdot\hat{\mathbf{n}} \end{aligned} \tag{7}$$

and $\hat{\mathbf{t}}$ are surface tractions, $\hat{\mathbf{n}}$, is the unit surface normal, and $\overline{q}^{(i)}$ is the charge per unit area of the i-th piezoelectric layer. The total charge $q_{piezo}^{(i)}$ produced by the piezoelectric layer material is then:

$$q_{piezo}^{(i)} = \int_S \overline{q}^{(i)}\mathrm{d}S \tag{8}$$

where the integration is over the in-plane surface area. See Marinkovic et al. (2007) for a similar treatment of the coupled piezoelectric equations.

In the electrode electrical conduction model only in-plane conduction is considered on a per-layer basis. The field equations for each electrode layer are developed using Maxwell's equations under quasi-static assumptions:

$$\nabla\cdot\mathbf{D}^{(i)} = \rho_e^{(i)} \tag{9}$$

$$\nabla\times\mathbf{H}^{(i)} = \mathbf{J}_f^{(i)} + \dot{\mathbf{D}}^{(i)} \tag{10}$$

with charge density ρ_e, magnetic field $\mathbf{H}$, and free current density $\mathbf{J}_f$. The constitutive law (Ohm's law) for electric conduction is:

$$\mathbf{J}_f^{(i)} = \sigma^{(i)}\mathbf{E}_e^{(i)} \tag{11}$$

with conductivity $\sigma^{(i)}$. Assuming an irrotational electric field such that $\mathbf{E}_e^{(i)} = -\nabla\phi^{(i)}$, integrating Equation (10) over the volume of the electrode, and combining with Equations (9) and (11), yields:

$$\dot{q}_{electrode}^{(i)} = \int \dot{\rho}_e^{(i)}\mathrm{d}V = \int \nabla\cdot\sigma^{(i)}\nabla\phi^{(i)}\mathrm{d}V \tag{12}$$

where $q_{electrode}^{(i)}$ is the total charge in the i-th electrode.

The final sub-model, the electrical circuit, is assumed to be linear and can be generalized as a RLC circuit with a series resistance R, capacitance C, and inductance L subject to a potential difference $\Delta\phi$. The circuit dynamics are described by:

$$\Delta\phi = \frac{1}{C}q_{circuit} + R\dot{q}_{circuit} + L\ddot{q}_{circuit} \tag{13}$$

where $q_{circuit}$ is the electric charge.

The equations of the three sub-models are combined by common Dirichlet boundary conditions and by the conservation of charge within the system:

$$q_{piezo} + q_{electrode} + q_{circuit} = 0 \tag{14}$$

which depends on the connectivity of the sub-models and combines Equations (8), (12), and (13), integrated in time assuming a time-harmonic response, to fully couple the piezoelectric harvesting structure, the electrodes, and the electric circuit.

Finite Element Formulation

We use the finite element method to discretize the equations for the electromechanics of the piezoelectric structure as well as the electrodynamics of the electrodes, while for the circuit we use a lumped parameter model. A four-node layered finite element is used where the layers may consist of either pure structural, piezoelectric, or electrode layers. The structural layers are built from four overlapping composite triangular elements (Hemez, 1994) composed of coupled 9-dof assumed natural deviatoric strain membrane (Felippa, 2003) and 9-dof bending (Militello and Felippa, 1991) triangular elements, resulting in 24 structural degrees of freedom per element. The piezoelectric layers use the same structural components coupled to the electric field via piezoelectric coupling (Marinkovic et al., 2007). In the formulation of the layered element, the middle in-plane strains, curvatures, and electric field are assumed constant and integration through the thickness is performed in a piece-wise manner using constant constitutive properties for each layer (Hemez, 1994). An arbitrary number of potential degrees of freedom may exist per node through the thickness, allowing for multiple, independent piezoelectric layers. Figure 2 illustrates an example layer configuration showing the location of potential degrees of freedom on a layer basis and the linear interpolation of potential through the thickness.

Under time harmonic assumptions ($\mathbf{u} = \mathbf{u}_e e^{i\omega t}, \phi = \boldsymbol{\phi}_e e^{i\omega t}$), with excitation frequency ω, the resulting piezoelectric finite element system with structural damping can be written as:

$$\begin{aligned} -\omega^2\mathbf{M}_e\mathbf{u}_e + i\omega\mathbf{C}_e\mathbf{u}_e + \mathbf{K}_e\mathbf{u}_e + \boldsymbol{\Theta}_e\boldsymbol{\phi}_e &= \mathbf{f}_e \\ \boldsymbol{\Theta}_e^T\mathbf{u}_e + \mathbf{C}_p\boldsymbol{\phi}_e &= \mathbf{q}_e \end{aligned} \tag{15}$$

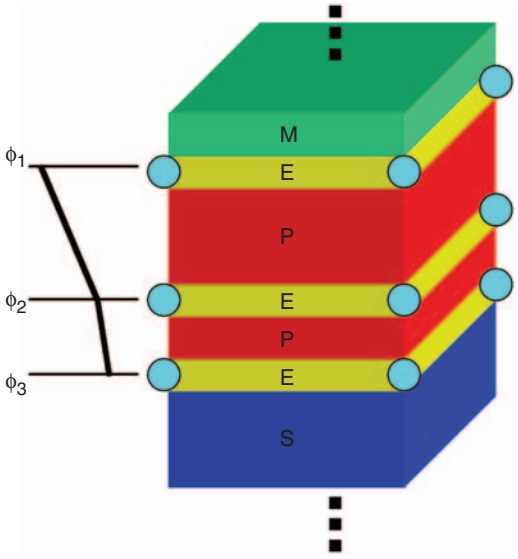

Figure 2. *An example construction of a piezoelectric layered element composed of (S) structural, (P) piezoelectric, (E) electrode, and (M) mass layers. An arbitrary number of potential degrees of freedom ϕ, marked by blue circles, may exist through the thickness.*

where $\mathbf{M}_e, \mathbf{C}_e, \mathbf{K}_e, \mathbf{\Theta}_e, \mathbf{C}_p, \mathbf{u}_e, \boldsymbol{\phi}_e, \mathbf{f}_e, \mathbf{q}_e$ are the elemental mass, damping, stiffness, piezoelectric coupling, and capacitance matrices, with the elemental nodal displacement, potential, force, and charge vectors.

The electrode layers conduct electricity in the plane of the element between voltage degrees of freedom of the same electrode layer with finite conductivity as described by Equation (12). Each electrode layer is discretized with a four-node bi-linear finite element (Bathe, 2007), which when combined under time harmonic assumptions yields:

$$i\omega\left(\frac{-1}{\omega^2}\mathbf{\Psi}_e\right)\boldsymbol{\phi}_e = \mathbf{q}_e \tag{16}$$

where $\mathbf{\Psi}_e$ is the elemental electrode conduction matrix for all the electrodes.

The time-harmonic electric circuit Equation (13) can be written as:

$$\left(-\omega^2\mathbf{R}_e^{\mathrm{M}} + i\omega\mathbf{R}_e^{\mathrm{C}} + \mathbf{R}_e^{\mathrm{K}}\right)\boldsymbol{\phi}_e = \mathbf{q}_e \tag{17}$$

where:

$$\begin{aligned}
\mathbf{R}_e^{\mathrm{M}} &= \frac{L}{\left(\frac{1}{C} - \omega^2 L\right)^2 + (\omega R)^2}\mathbf{R}^{\mathrm{I}},\\
\mathbf{R}_e^{\mathrm{C}} &= \frac{-R}{\left(\frac{1}{C} - \omega^2 L\right)^2 + (\omega R)^2}\mathbf{R}^{\mathrm{I}},\\
\mathbf{R}_e^{\mathrm{K}} &= \frac{\frac{1}{C}}{\left(\frac{1}{C} - \omega^2 L\right)^2 + (\omega R)^2}\mathbf{R}^{\mathrm{I}}
\end{aligned} \tag{18}$$

and $\mathbf{R}^{\mathrm{I}}$ connects the potential field degrees of freedom in the lumped parameter formulation. Using Equation (14) to connect Equations (15), (16), and (17) yields the final system of equations:

$$\tilde{\mathbf{K}}\begin{pmatrix}\mathbf{u}\\ \boldsymbol{\phi}\end{pmatrix} = \begin{bmatrix}\mathbf{K}_{11} & \mathbf{K}_{12}\\ \mathbf{K}_{21} & \mathbf{K}_{22}\end{bmatrix}\begin{pmatrix}\mathbf{u}\\ \boldsymbol{\phi}\end{pmatrix} = \begin{pmatrix}\mathbf{f}\\ 0\end{pmatrix} \tag{19}$$

where:

$$\begin{aligned}
\mathbf{K}_{11} &= -\omega^2\mathbf{M} + i\omega\mathbf{C} + \mathbf{K}\\
\mathbf{K}_{12} &= \mathbf{\Theta}\\
\mathbf{K}_{21} &= \mathbf{\Theta}^T\\
\mathbf{K}_{22} &= -\omega^2\mathbf{R}^{\mathrm{M}} + i\omega\left(\frac{-1}{\omega^2} + \mathbf{R}^{\mathrm{C}}\right) + \left(\mathbf{R}^{\mathrm{K}} + \mathbf{C}_p\right)
\end{aligned} \tag{20}$$

for which the matrices are assembled in the global sense with global system matrix $\tilde{\mathbf{K}}$. The mechanical response of the structure is described by $\mathbf{K}_{11}$, which changes with the layout of materials both layer-wise and in the plane of the plate structure. The matrices $\mathbf{K}_{12}$ and $\mathbf{K}_{21}$ are the piezoelectric coupling matrices, which couple the structural and electrical responses and vary with piezoelectric material layout. The dynamics of the electrical response are provided by the interaction of the circuit matrices $\mathbf{R}^{\mathrm{M}}$, $\mathbf{R}^{\mathrm{C}}$, and $\mathbf{R}^{\mathrm{K}}$ with the piezoelectric capacitance matrix $\mathbf{C}_p$, which varies with the material layout, and the electrode matrix $\mathbf{\Psi}$, which varies with the electrode conductivity and topology.

Topology Optimization Formulation

We formulate design problems by a general nonlinear program with objective z, inequality constraints g_j, and equality constraints h_k being twice differentiable functions of design variables s_i:

$$\begin{aligned}
&\max_{s_i} z(s_i, \mathbf{u}(s_i), \boldsymbol{\phi}(s_i)) \quad i = 1 \ldots n_s\\
&\text{s.t. } \tilde{\mathbf{K}}(s_i)\begin{pmatrix}\mathbf{u}(s_i)\\ \boldsymbol{\phi}(s_i)\end{pmatrix} = \begin{pmatrix}\mathbf{f}\\ 0\end{pmatrix}\\
&g_j(s_i) \le 0 \qquad j = 1 \ldots n_g\\
&h_k(s_i) = 0 \qquad k = 1 \ldots n_h\\
&\underline{s_i} \le s_i \le \overline{s_i}
\end{aligned} \tag{21}$$

where there are n_s design variables bounded by the lower and upper box constraints $\underline{s_i}$ and $\overline{s_i}$, respectively, n_g inequality constraints and n_h equality constraints. The system matrix is a direct function of the design variables, $\tilde{\mathbf{K}} = \tilde{\mathbf{K}}(s_i)$, and the solution vectors are implicit functions of the design variables, $\mathbf{u} = \mathbf{u}\left(\tilde{\mathbf{K}}(s_i)\right), \boldsymbol{\phi} = \boldsymbol{\phi}\left(\tilde{\mathbf{K}}(s_i)\right)$ Following a material-based topology optimization approach, the material properties of one or a group of

finite elements are defined as smooth functions of the design variables s_i such that the lower bound $\underline{s_i}$ corresponds to one particular material and the upper bound $\overline{s_i}$ to a second material. Intermediate values $\underline{s_i} < s_i < \overline{s_i}$ correspond to an artificial composite material. In general, the interpolation of the material properties as a function of the design variables is chosen such that the optimization problem (21) converges to a solution with all optimization variables being at or near the upper and lower bounds. For the design of piezoelectric energy harvesters studied in this article, we have observed that the nature of the optimization drives the optimization variables to the upper/lower bounds. Reasons for this behavior will be discussed later. Therefore we use simple linear interpolations to define the mass density, the stiffness coefficients, the piezoelectric coupling constant, as explicit functions of the optimization variables:

$$\begin{aligned} \rho^{(i)} &= \left(\rho_{(1)} - \rho_{(0)}\right)s_i + \rho_{(0)} \quad 0 \le s_i \le 1 \\ Q^{(i)}_{k,l} &= \left(Q_{(1)k,l} - Q_{(0)k,l}\right)s_i + Q_{(0)k,l} \quad i = 1 \ldots (n_s - 1) \\ e'_{31}(i) &= \left(e'_{(1)31} - e'_{(0)31}\right)s_i + e'_{(0)31} \end{aligned} \tag{22}$$

where the subscripts 0 and 1 denote the lower and upper bounds for the variable corresponding to design variable values of $s_i = [0,1]$. It is possible with our framework, but not explored in our examples, to additionally treat the electrode conductivity as variable as a means to design the layout of electrodes on the piezoelectric layers.

When the circuit resistance is also varied we use a nonlinear interpolation function as follows:

$$R = R_{(0)} \exp\left(\ln\left(\frac{R_{(1)}}{R_{(0)}}\right)s_j\right) \quad j = n_s \tag{23}$$

This interpolation approach counteracts the large influence of the resistance on the energy harvesting performance that dominates over the influence of the material parameters described above, and thus mitigates numerical problems when solving the optimization problem (21).

Note that in our problem-specific formulation the dielectric permittivity of the piezoelectric layer is not varied with the other properties of the piezoelectric layer. This is done as a matter of stabilization of the optimization method to overcome scaling differences between the inherent piezoelectric and electrical circuit problems that appear in the optimization problem (21). In our study we investigate only a purely resistive external circuit, although the piezoelectric material surrounded by electrodes acts as a capacitor thereby making the whole system act like an RC circuit. In standard RC circuits, the maximum power is dissipated for an oscillation frequency $\omega = 1/(\mathrm{RC})$. However, finding the optimal resistance and capacitance in the case of piezoelectric harvesting is not as easy as satisfying the RC-circuit condition, as demonstrated by Erturk and Inman (2008d) and Renno et al. (2009), although the behavior is similar. In general, the resistance and capacitance need to be tuned simultaneously to reach the optimal circuit power for the harvester. This can be done by adding or removing piezoelectric material to change the capacitance and/or by directly changing the circuit resistance. While in general both types of modifications are needed to achieve an optimal performance, the optimal circuit problem dominates over the optimal piezoelectric topology problem driving the optimization problem to a local minimum and resulting in a piezoelectric layer that fully covers the plate. To overcome this issue we keep the dielectric permittivity of the piezoelectric layer constant, which yields a constant system capacitance, regardless of piezoelectric layout. To realize the optimal design, the fictitious contributions of the piezoelectric layer to the capacitance are translated into to an external capacitor in parallel with the piezoelectric plate. As a result, in optimizing the piezoelectric layout, the capacitance value of this external capacitor is also optimized at the same time, albeit indirectly. This procedure effectively isolates the piezoelectric and electrical circuit problems from each other, thereby allowing the piezoelectric material layout to change without changing the properties of the RC-like circuit.

Using the formulation (21), a broad class of design problems pertaining to piezoelectric energy harvesting can be formulated and solved. Owing to the large number of design variables, we solve the optimization problem (21) by gradient-based techniques requiring the calculation of gradients of the objective and constraints with respect to the design variables. The derivative of the objective, for example, can be expanded as follows:

$$\begin{aligned} \frac{\mathrm{d}z(s_i, \mathbf{u}(s_i), \boldsymbol{\phi}(s_i))}{\mathrm{d}s_i} &= \frac{\partial z}{\partial s_i} + \left(\frac{\partial z}{\partial \boldsymbol{\phi}} + \frac{\partial z}{\partial \tilde{\mathbf{K}}}\frac{\partial \tilde{\mathbf{K}}}{\partial \boldsymbol{\phi}}\right)\frac{\mathrm{d}\boldsymbol{\phi}}{\mathrm{d}s_i} \\ &\quad + \left(\frac{\partial z}{\partial \mathbf{u}} + \frac{\partial z}{\partial \tilde{\mathbf{K}}}\frac{\partial \tilde{\mathbf{K}}}{\partial \mathbf{u}}\right)\frac{\mathrm{d}\mathbf{u}}{\mathrm{d}s_i} \\ &= \frac{\partial z}{\partial s_i} - \left(\frac{\partial z}{\partial \boldsymbol{\phi}} + \frac{\partial z}{\partial \tilde{\mathbf{K}}}\frac{\partial \tilde{\mathbf{K}}}{\partial \boldsymbol{\phi}}\right)\tilde{\mathbf{K}}^{-1}\frac{\partial \tilde{\mathbf{K}}}{\partial s_i}\boldsymbol{\phi} \\ &\quad - \left(\frac{\partial z}{\partial \mathbf{u}} + \frac{\partial z}{\partial \tilde{\mathbf{K}}}\frac{\partial \tilde{\mathbf{K}}}{\partial \mathbf{u}}\right)\tilde{\mathbf{K}}^{-1}\frac{\partial \tilde{\mathbf{K}}}{\partial s_i}\mathbf{u} \end{aligned} \tag{24}$$

Which can be evaluated using either the direct or adjoint method (Haug et al., 1986).

Formulation of a Specific Objective for Piezoharvesting

The formulation of the optimization problem (21) is quite general and as such can be used to solve a wide range of design problems regarding piezoelectric energy harvesters. In the examples that follow we apply it to a more restrictive suite of problems that involve determining the layout of piezoelectric patches on an elastic substrate to maximize the harvested power for a given operating frequency (Figure 3). In addition, we determine the optimal resistance of the harvesting circuit. To this end we formulate the objective function as:

$$z = \frac{|\Delta\phi|^2}{2R} \tag{25}$$

which is a measure of the average power dissipated by the resistor. The flexibility of our methodology also admits other objective functions, such as volume- and mass-specific power density, which may be more appropriate in some situations; but these are not explored here. The gradients of the objective can be written as:

$$\frac{\mathrm{d}z(s_i)}{\mathrm{d}s_i} = \frac{\partial z}{\partial R}\frac{\mathrm{d}R}{\mathrm{d}s_i} + \frac{\partial z}{\partial \phi}\frac{\mathrm{d}\phi}{\mathrm{d}s_i} = -\frac{|\Delta\phi|^2}{2R^2}\frac{\mathrm{d}R}{\mathrm{d}s_i} + \frac{1}{R}\mathrm{Re}\left[\phi^*\tilde{\mathbf{K}}^{-1}\frac{\partial\tilde{\mathbf{K}}}{\partial s_i}\phi\right]. \tag{26}$$

We evaluate the gradients (26) by the adjoint method. In the examples studied in the following no inequality or equality constraints are considered. Also, no gradient filtering or penalization techniques are used, although these augmentations can be easily included into our computational framework. We solve the optimization problem (25) with a sequential quadratic programming algorithm (Schittkowski, 1985).

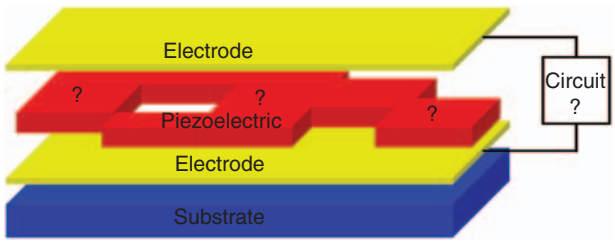

Figure 3. *Illustration of the problem setup using topology optimization to determine the layout of the piezoelectric layer and the circuit parameters.*

ANALYSIS DEMONSTRATION AND MODEL VALIDATION

We validated our numerical model by analyzing two problems where analytical solutions and/or experimental results are given in the literature. The first problem is a cantilever beam harvester (Erturk and Inman, 2008b, c, 2009; Erturk et al., 2009) and the second problem a piezoelectric circular plate (Kim et al., 2005a, b). In both of these cases, fully covered cantilevers and plates were considered as well as special cases where only part of the structure was covered by a piezoelectric patch and/or an electrode. In all cases we obtained excellent agreement between our simulation results and the analytical solutions and/or experimental results reported in these papers. Two illustrative examples are shown here.

Cantilever Beam

The first validation example follows the study of Erturk and Inman (2009) who use a vibrating bimorph cantilever beam connected to a circuit for energy harvesting. They develop an analytical model that compares favorably with experimental data. Here we compare their validated analytical model to our finite element model for the same setup thereby validating our model as well. The setup for the cantilever bimorph consists of 0.14 mm thick brass beam surrounded by 0.26 mm PZT-5A piezoelectric layers and two 0.006 kg tip masses. The beam is 50.8 mm long and 31.8 mm wide. The material properties can be found in Erturk and Inman (2009). In order to reproduce their results derived from beam theory with our plate formulation we use a Poisson's ratio of zero in our calculations.

The two piezoelectric layers are connected in series with each other and with an external circuit consisting of a resistor of variable resistance as shown in Figure 4. Our finite element model consists of a 25×15 element mesh of the layered piezoelectric plate elements described earlier. A structural layer is sandwiched between two piezoelectric layers. At the bottom and top, electrode layers with a conductivity of $1.0\mathrm{e}4\,\Omega^{-1}$ are placed; the conductivity is large enough to model nearly perfect conduction, but small enough to prevent numerical issues due to ill-conditioned system matrices. The connections between electrodes are modeled with resistive elements, one with the load resistance and the other with a negligible resistance to connect the two inner layers. Lumped masses are included at the beam tip and mass proportional damping of 2.7% is applied, as determined from Erturk and Inman's experiments. Frequency sweeps are performed for harmonic base excitation and the output power through the resistor is calculated for resistivities of 1, 33, and 470 kΩ. Figure 5 shows the power frequency response functions (FRFs)

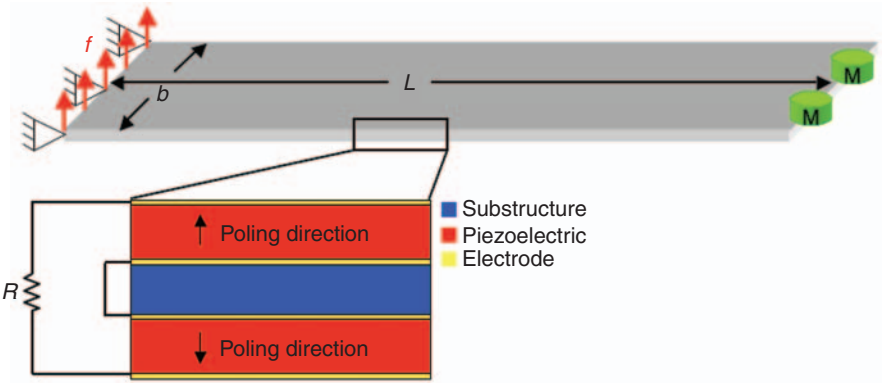

Figure 4. *Schematic of a cantilever bimorph used for validation of our modeling approach.*

plotting the output power normalized to the square of acceleration, g^2, over the excitation frequency. The results are in excellent agreement with Erturk and Inman's analytical solution. The largest output power is obtained for 33 kΩ, suggesting that there is an optimal resistance for the external circuit that maximizes the output power.

Clamped Circular Plate

In the second example we consider the static deformation of a $R_2 = 25$ mm diameter circular plate that is clamped at the outer edge and consists of a 0.127 mm thick piezoelectric PZT-5H layer on a 0.508 mm thick aluminum substrate. The material properties are given in Table 1. An external static pressure is applied to one side of the plate and the resulting open circuit voltage is calculated. This problem can be considered a special case of our dynamic finite element model (19) such that $\omega \to 0$ and $R \to \infty$. In order to increase the voltage generated by the plate, the material in the PZT-5H layer is arranged such that the piezoelectric polarization (polarity) changes sign/direction (i.e., the coupling constant changes sign) at R_1. Figure 6(a) shows the problem setup. This problem was studied by Kim et al. (2005a, b), who provided an analytical solution and carried out supporting experiments. Our finite element model consists of a mesh of 18,000 elements, which was determined to be adequate by a mesh refinement study. Our finite element results are in good agreement with the published experimental data as shown in Table 2.

To study the influence of the layout of the piezoelectric layer on the performance of the structure, we vary the radius R_1 and plot the open circuit voltage as a function of R_1/R_2 in Figure 6(b). The open circuit voltage is maximum for $R_1/R_2 = 0.7$. Plotting the mean curvature (arithmetic mean of in-plane curvatures) as a function of radius in Figure 6(c) shows that curvature changes sign at $r/R_2 = 0.7$. To avoid charge and voltage cancellation, the polarity of the piezoelectric material needs to switched at $R_1/R_2 = 0.7$. This finding

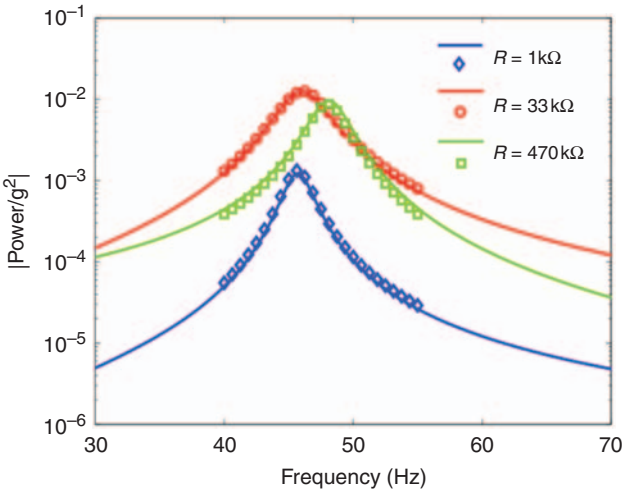

Figure 5. *Power FRF for a piezoelectric bimorph cantilever beam for resistances of 1, 33, and 470 kΩ. Finite element calculations are shown as open symbols while the analytical solutions are shown as solid lines.*

is consistent with Erturk and Inman (2008b) and Erturk et al. (2009).

Instead of determining the optimum value of R_1/R_2 through a parameter sweep, we use this example to test our design methodology and let the optimizer find the optimum material distribution. The optimization problem is defined to maximize the open circuit voltage by finding the optimal distribution of two materials that differ only in the sign of their piezoelectric coupling coefficients. The design variables interpolate the piezoelectric coupling constant linearly from a positive value to a negative value (i.e., it is either poled upward or downward). While for this axisymmetric problem it would be sufficient to consider only the variation of polarization as a function of radius, in our setup of the optimization problem the design variables define the polarity in the piezoelectric layer independently in each element. Figure 6(d) shows this optimal distribution which has a corresponding optimal open circuit

Table 1. Material properties used in examples.

	Mass density	Stiffness properties	Piezoelectric properties
Piezoelectric (PZT-5H)	$\rho = 7500\ kg/m^3$	$c^E_{11} = c^E_{22} = 127$ GPa $c^E_{12} = 80.2$ GPa $c^E_{13} = c^E_{23} = 84.7$ GPa $c^E_{33} = 117$ GPa	$e_{31} = -6.62$ N/C $e_{33} = 23.2$ N/C $\varepsilon^S_{33} = 1.27e-8$ F/m
Aluminum substrate	$\rho = 2700$ kg/m^3	$E = 73.0$ GPa, $\nu = 0.33$	
Mass layer	$\rho = 7500$ kg/m^3	$E = 0$ GPa	

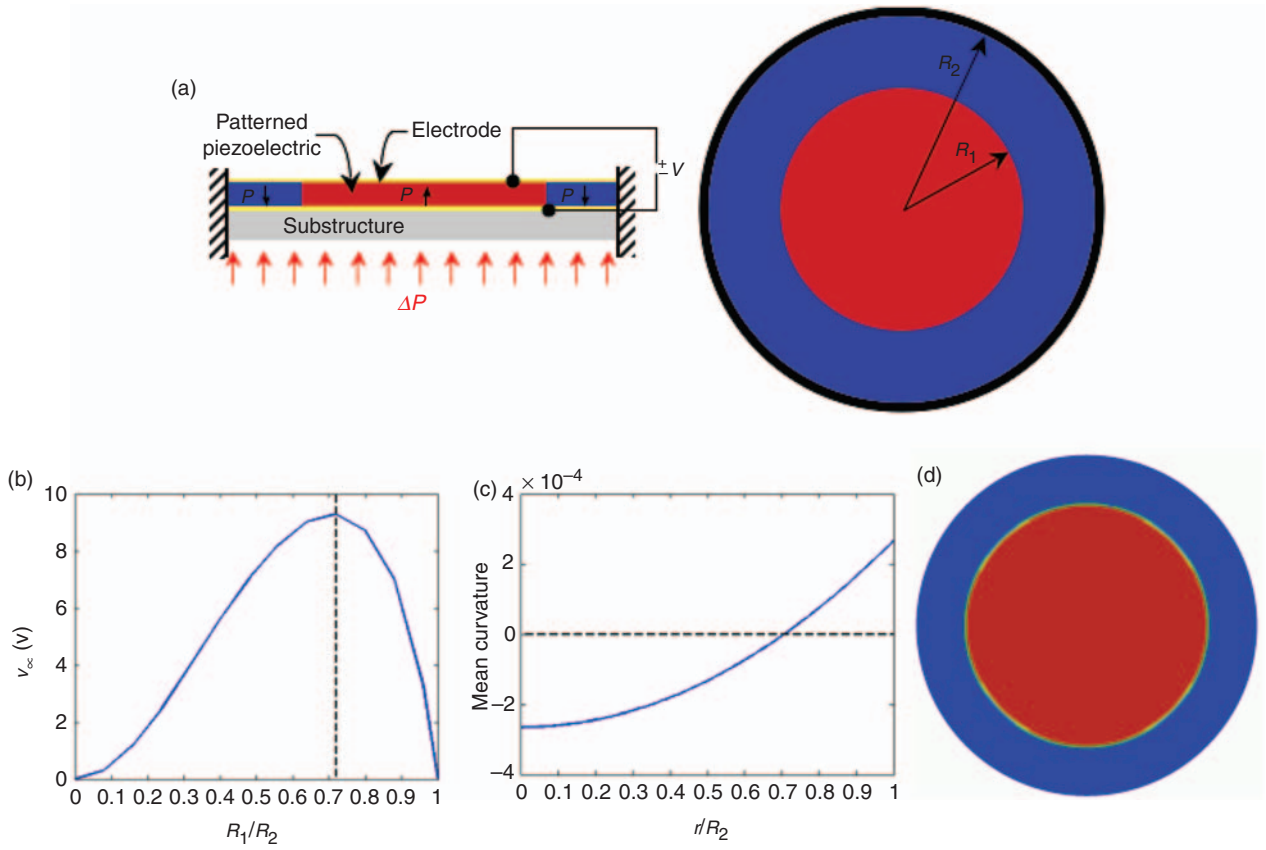

Figure 6. *(a) Problem setup of a circular plate with a pressure load, (b) open circuit voltage as a function of polarization reversal radius, (c) mean curvature of the plate as a function of radius, (d) optimal piezoelectric polarization layout using topology optimization (red – positive polarization, blue – negative polarization).*

voltage of 9.31 V at about $R_1/R_2 = 0.71$ (an estimate because of the finite element discretization), which correlates well with the analytical optimal solution provided by Kim et al. (2005a).

It is noteworthy that the optimized material distribution in Figure 6(d) lacks any intermediate design variables i.e., $s_i \neq 0$ or 1. All optimization variables converge to their upper or lower limit without penalizing intermediate values. The clear spatial separation of the material distribution can be explained by the desire to have all regions of piezoelectric material produce as much charge as possible. As the charge generation depends on the sign of the curvature, the material domains are clearly separated and the design variables are at their extreme values yielding the maximum piezoelectric coupling coefficients.

Table 2. Generated V_{OC} (in V) vs R_1/R_2 for $\Delta P = 9.65$ kPa.

R_1/R_2	Experiment	Analysis
0.40	5.31 ± 0.014 5.61 ± 0.014	5.61
0.72	8.84 ± 0.039 9.26 ± 0.010	9.29

In this example, the layout of the piezoelectric layer has a negligible effect on structural response due to

static pressure loading. The regions with positive and negative curvature can be determined and, neglecting small piezoelectric effects, the layout of the piezoelectric layer can be aligned with the curvature distribution. We show in the following section that this procedure is not applicable to problems where the structural response depends on the layout of piezoelectric material. In this case our optimization approach provides a useful tool to find the optimum distribution of piezoelectric material.

APPLICATION EXAMPLES

In this section we present four examples that demonstrate the capabilities of our approach. In particular we focus on a suite of examples that cannot yield solutions through analytical beam or plate analysis methods. We show how adding a piezoelectric energy harvesting layer can drastically change the response of a system and that simply placing material in regions of positive or negative curvature will not necessarily yield a design that effectively harvests energy. Optimal designs that overcome this problem using our methodology are presented and discussed. We then show how the parameters of the harvesting circuit, namely the resistance, affect the power output of the energy harvesting system. This is followed by a study of how adding a mass layer with negligible stiffness to the structure changes the response and the optimal design of the plate structure and how it can improve results more than optimizing the piezoelectric layer alone. The final example demonstrates that our technique is applicable to a curved base structure and illustrates the versatility of our approach as not only a design tool, but also as a tool for investigating physical trends associated with optimally designed structures. Our intent is to show how our approach and tools can be used to explore the general behavior and develop overarching principles through the study of a suite of particular problems in piezoelectric energy harvesting.

Clamped Square Plate – Thickness Effects

Here we consider the design of a $10 \times 10\,\text{cm}$ clamped square plate as shown in Figure 7. The plate is clamped at the middle two-fifths of one side and is subject to a harmonic excitation of 575 Hz at the clamped location normal to the plane of the plate, actuated as a unit displacement. The objective of the example is to determine the optimal layout of piezoelectric material on top of a substrate such that the power dissipated by a constant $1\,\text{k}\Omega$ resistor is maximized. The initial design for the optimization problem is a plate fully covered with piezoelectric material. This optimization problem is solved for six different thickness ratios of piezoelectric to substrate materials. The piezoelectric is transversely isotropic PZT-5H with thicknesses of $h_p = [0.001, 0.025, 0.1, 0.2, 0.3, 0.5]\,\text{mm}$, while the substrate is aluminum with a constant thickness of $h_s = 1\,\text{mm}$. The material properties are given in Table 1. The finite element model is discretized into a 25×25 element mesh. It was found that for undamped structures, the sudden phase change in voltage and displacement at resonance creates a non-smooth optimization landscape that cannot be traversed efficiently by gradient-based algorithms. In order to alleviate this problem, as well as make it more practical, mass proportional damping of 1% is included in the problem.

The resulting optimal material layouts are shown in Figure 8. As the thickness ratio increases the optimal design gradually changes. The designs optimized for the largest and smallest thickness ratios significantly differ. For a thin piezoelectric layer the material layout in the piezoelectric layer closely matches the signs of the strain distribution computed for a plate without piezoelectric layer (Figure 8). With increasing thickness the material layout differs increasingly from this strain distribution as the piezoelectric layer adds stiffness and mass thereby changing the dynamic response of the structure.

In general, it cannot be guaranteed that the optimization problems considered in this study are convex and the optimization process converges to the global minimum. To address the latter issue, the optimization problems were tested for local optima by starting the optimization process from a number of random initial designs, all of which converged to the same solution. These mimina results suggest, but do not prove, that the optimization problem is globally convex and the solutions obtained are at least strong local minima.

The relationship between thickness ratio and optimal design is studied further by taking each piezoelectric pattern of Figure 8 (designs A–F), varying the piezoelectric thickness from $h_p/h_s = 0.001$–0.5, and computing the power generated in each case. These results are shown in Figure 9, where the output power for each design is normalized to the power output of the optimal design for that thickness ratio. For each thickness ratio the maximum power is produced by the design optimized for that thickness. This situation is not as intuitive as it might seem as evidenced by the non-monotonic behavior when moving away from the diagonal (which represents the family of optimal designs) in Figure 9, e.g., design D at $h_p/h_s = 0.5$ or design F at $h_p/h_s = 0.2$. The results also suggest an increasing sensitivity to design changes as thickness ratio increases, for example in the noticeable drop in power output between designs F and E at $h_p/h_s = 0.5$. Although the two designs have

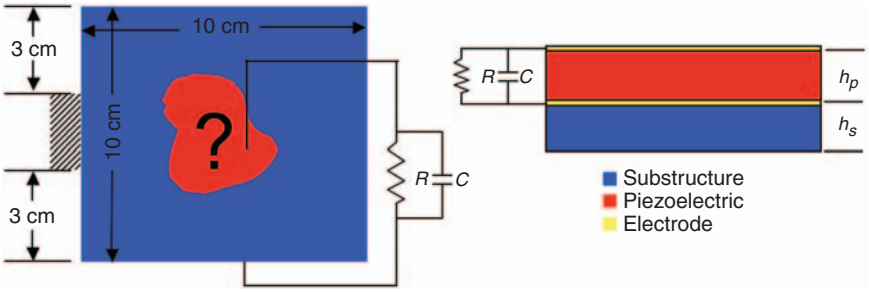

Figure 7. *Design problem setup of a square plate subject to harmonic loading.*

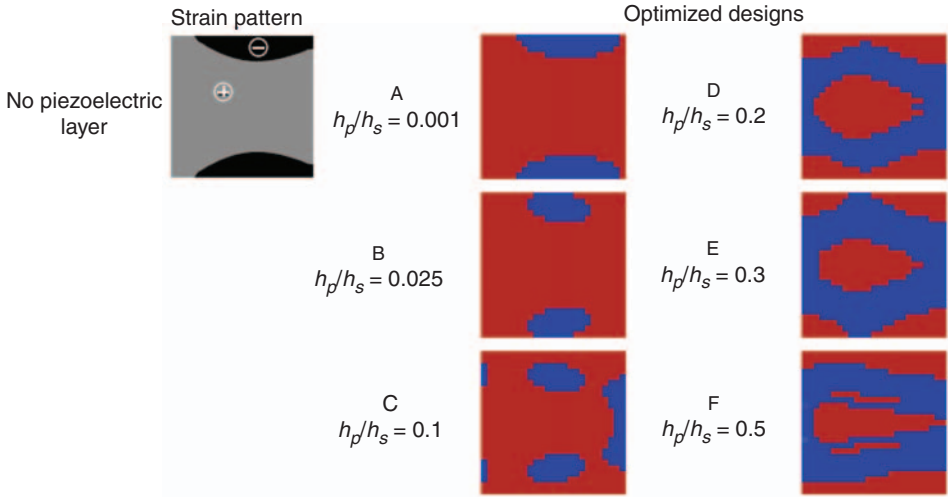

Figure 8. *Comparison of the strain pattern for a plate without a piezoelectric layer with the optimal distribution of piezoelectric material (red) on an aluminum substrate (blue) for six different ratios of piezoelectric to substrate thickness.*

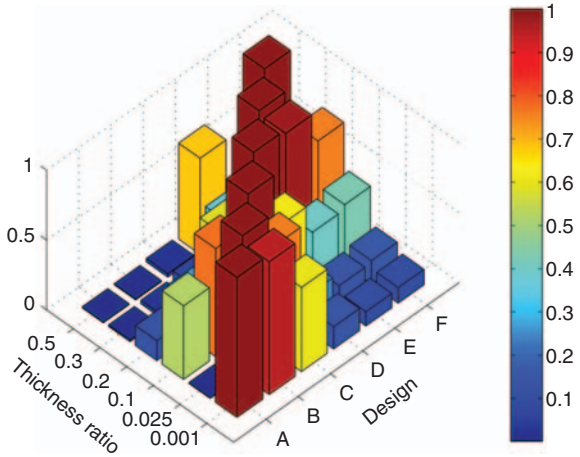

Figure 9. *Power output for each design at each thickness ratio. The power magnitude of each thickness ratio is normalized to the power of the optimal design at that thickness ratio.*

somewhat similar features, the power output is significantly different because of the change in structural response caused by the additional thickness of the piezoelectric layer.

The absence of intermediate design variables is also seen in this example, as was the case with the circular plate example. The difference here is that the structural properties change along with the coupling coefficient, while at the same time the structure is experiencing feedback from the external circuit. As a result, a complex interplay between structural response, charge production, and charge utilization occurs. Regardless of the complexity, the results suggest that for the objective function used the piezoelectric coupling coefficients converge to their extreme values thereby maximizing charge output.

Figure 10 shows FRFs of the output power encompassing the second through fourth modes for the fully covered and optimal plate designs for each of the thickness ratios. The FRFs for the fully covered plates show the general trend that an increase in thickness results in an increase in output power as well as a change in the response where the third mode shifts to lower frequencies. The driving frequency for this problem is consistently located between the second and third bending modes for these cases. For the optimal designs, the degree to which the FRF changes increases with

thickness ratio. As the piezoelectric layer constitutes a larger fraction of the total structural makeup the more its variation affects the overall structural response. For lower thickness ratios with less ability to change the structural response, the increase in output power is not caused by changes in the location of the natural frequencies, but the relative influence of the modes at the driving frequency. This is best seen for $h_p/h_s = 0.001$ and 0.025. As the thickness ratio increases, however, more freedom is allowed in the design to shift modes to different frequencies, specifically to move a mode to toward the driving frequency such that the driving frequency becomes a resonant frequency. This is indicated in Figure 10 by the gradual shifting of the third mode to the driving frequency with increased thickness ratio, whereas more freedom to move the modes allows for the third mode to get closer to the driving frequency. As such, designs E and F of Figure 8 are structures with natural frequencies at the driving frequency of 575 Hz and are akin to tuned cantilever beam harvesters typically used in energy harvesting applications, but without the need to change the shape or add an end mass.

In summary, these results show a strong influence of thickness ratio on the optimal layout of piezoelectric material on the plate. At larger thickness ratios the addition/removal of piezoelectric material significantly changes the mass and stiffness properties of the structure. In particular in the case that the piezoelectric material constitutes a significant proportion of the structure, the resulting material redistribution changes the structural modes in such a way that the structure simultaneously is 'tuned' to the driving frequency and prevents charge cancellation, Not only do these results demonstrate the need to treat the coupled piezoelectric layer as an integral part of the system and its structural response when considering the design of piezoelectric energy harvesters, they also demonstrate the manner in which topology optimization can overcome the limitations of other existing design methods to improve the power output of such devices.

Simultaneous Piezoharvester and Circuit Design

Here we consider the same edge-clamped square plate as in the previous example with the exception that the external circuit resistance is treated as a design variable along with the piezoelectric properties of the structure. In the previous example the electrical characteristics of the circuit were kept constant including the electrical capacitance of the system. As explained earlier, this is because the dielectric permittivity of the piezoelectric is not varied with its other properties, allowing for separation of the structural/material layout and electrical parts of the optimization problem. In this problem, the plate again is optimized for the six different thickness ratios with the same harmonic excitation of 575 Hz. The optimization problem is started from an initial design with a fully covered piezoelectric layer. The material layout is kept variable along with the resistor to allow for simultaneous structure and circuit design.

The material distributions converge to same layouts as obtained previously for a fixed resistivity of 1.0 kΩ and shown in Figure 8. Figure 11 shows the power output of the final optimized material layouts as a function of circuit load resistance as well as the individual optimized values for those designs at $R = 1.0\,\text{k}\Omega$ and the optimal resistances. This figure reveals the RC circuit-like behavior of power output as a function of resistance and shows that the final harvesting circuit resistance

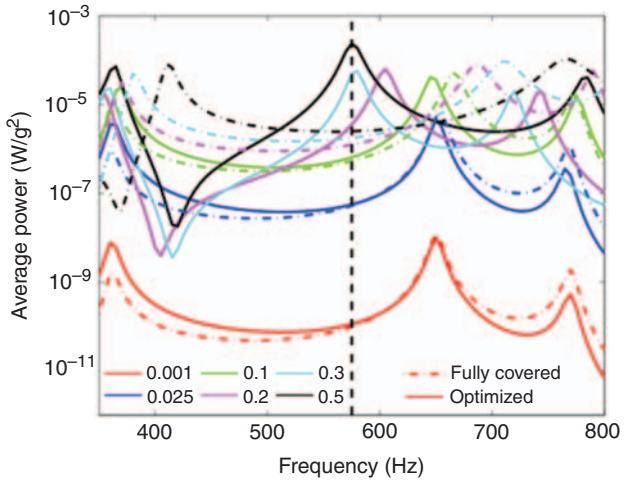

Figure 10. *Power FRFs of both the fully covered (dots) and optimized designs (solid) for each of the thickness ratios. The vertical dashed line is the frequency at which the designs are optimized; it is located between the second and third modes for all of the fully covered plates.*

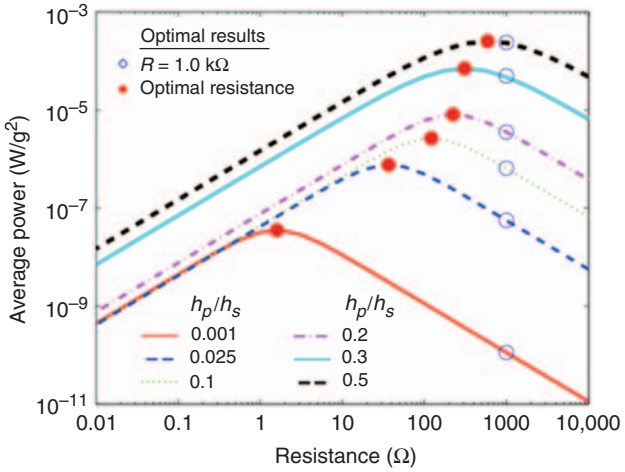

Figure 11. *Power output as a function of resistance for all six thickness ratios including the optimal solutions obtained with* R = *1kΩ (open circles) and with the resistance as an optimization variable as well (closed circles).*

obtained via optimization coincides with the maxima of those curves. These data are also listed in Table 3, which provides a comparison of power output for all the designs including plates fully covered with piezoelectric. The data show that, while for small thickness ratios the optimal piezoelectric layout contributes little to improving the power output, but as the thickness ratio increases the layout becomes increasingly important. This is particularly evident in the $h_p/h_s = 0.5$ design where the power output is improved by over 75 times. Also noted are that the optimal resistances between the fully covered and optimal designs are different even though the system capacitance is the same. This indicates, along with the calculated data shown in Table 4, that the optimal resistance obtained by applying the optimal circuit condition for an RC circuit does not correspond well with the results from our optimization. This finding is in agreement with those of Erturk and Inman (2008d) and shows that obtaining the optimal parameters for the harvesting circuit is equally important as finding the proper structural design to provide that power, and that our approach yields both.

Optimization with a Mass Load

In applications of piezoelectric cantilever beam harvesters, it is commonplace to tune the first resonant frequency of the beam to the primary ambient frequency to which it is exposed, thereby maximizing the transferable energy. This can be accomplished by altering the length or width of the beam or adjusting material parameters, but in practice this is often most easily achieved by adding a mass to the tip of the beam, which is particularly useful for manufactured beams with material properties and dimensions that are unalterable. Here we illustrate how our topology optimization can be used not only to determine the layout of the piezoelectric material, but also to determine how to spatially distribute a layer of nonstiffening mass to maximize the power output. The problem setup is the same as that for the first example with $R = 1.0\,\text{k}\Omega$, a thickness ratio $h_p/h_s = 0.1$, and an excitation frequency of 575 Hz, but with an extra mass layer of thickness 0.1 mm on top as shown in Figure 12. The density of the mass layer is the same as that of the piezoelectric. There is no constraint on placement of the mass layer so it is possible that extra mass can be placed where there is no piezoelectric to support it, although this has little effect on the system response. These results can be used to determine the placement of an array of lumped masses or of a high density/low stiffness layer to improve harvester performance. Our formulation could also be easily modified to allow for placing larger mass lumps in specific locations, similar to what is done in practice, but this option is not studied here.

The optimal material layouts of both the piezoelectric and mass layer are shown in Figure 12. Interestingly, the optimal layout of the piezoelectric material bears no resemblance to the optimal designs without the mass layer (specifically design C in Figure 8). The power FRFs of this and design C of Figure 8 are shown in Figure 13. In both cases, for the optimum designs, the third mode is shifted toward the driving frequency. As was shown before, the optimal layout of the piezoelectric layer alone is not sufficient to move the third mode all

Table 3. Power output for various designs at a frequency of 575 Hz.

h_p/h_s	Fully covered with $R = 1.0\,\text{k}\Omega$ (W/g^2)	Fully covered with variable R (W/g^2)	Fully covered optimal resistance (Ω)	Optimized design with $R = 1.0\,\text{k}\Omega$ (W/g^2)	Optimized design with variable R (W/g^2)	Optimized design optimal resistance (Ω)
0.001	9.83e-11	3.08e-8	1.59	1.13e-10	3.54e-8	1.60
0.025	5.29e-8	7.34e-7	35.9	5.60e-8	7.62e-7	36.6
0.1	5.37e-7	2.36e-6	114	6.49e-7	2.65e-6	121
0.2	1.25e-6	3.25e-6	198	3.55e-6	8.09e-6	223
0.3	1.78e-6	3.39e-6	282	4.95e-5	7.02e-5	309
0.5	2.51e-6	3.28e-6	465	2.39e-4	2.52e-4	591

Table 4. Calculated and optimal circuit resistances.

h_p/h_s	Calculated piezoelectric system capacitance (F)	Calculated optimal resistance $R = 1/\omega C$ (Ω)	Fully covered optimal resistance (Ω)	Optimized design optimal resistance R (Ω)
0.001	1.27E-4	2.18	1.59	1.60
0.025	5.08E-6	54.5	35.9	36.6
0.1	1.27E-6	218	114	121
0.2	6.35E-7	435	198	223
0.3	4.23E-7	654	282	309
0.5	2.54E-7	1090	465	591

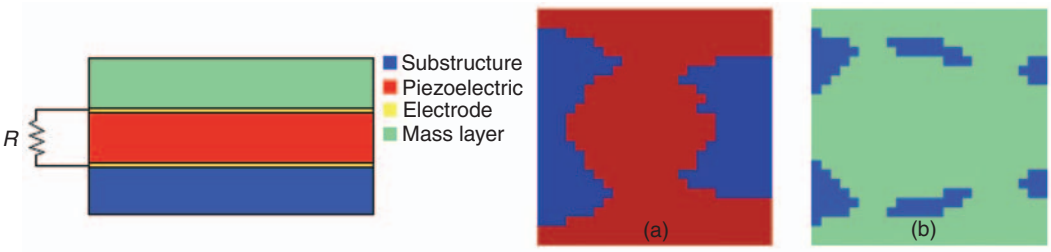

Figure 12. *Through-thickness setup for a problem with a mass layer is the same as the flat plate problem but with a to-be-optimized layer of non-stiffening mass on the top. Optimal distribution of material in the (a) piezoelectric layer (red) and (b) mass layer (green).*

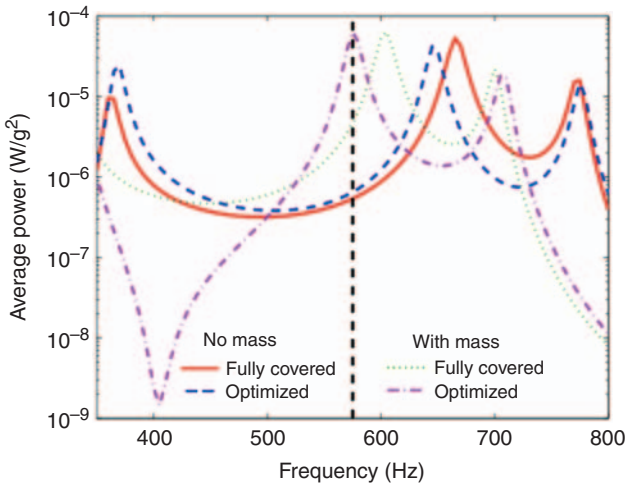

Figure 13. *Power FRFs for fully covered and optimized designs with and without the added mass layer. The optimal design without the mass layer is the same as in Figure 8 design C.*

the way to the driving frequency at this thickness ratio, but the addition of the mass layer provides enough design freedom to achieve this in the optimal design. Indeed the added mass layer actually gives more freedom than the optimal structure with this same thickness ratio (i.e., $h_p/h_s = 0.2$, Figure 8, design C) and mass. The power output for this design at $R = 1.0\,\text{k}\Omega$ is $P = 6.34\text{e-}5\,\text{W/g}^2$ which is greater than the output for a piezoelectric layer twice as thick shown in Table 3. This indicates that, for our example at least, optimizing an added mass layer in addition to the piezoelectric layer is more effective than increasing the thickness of a single piezoelectric layer and optimizing. The primary reasons for this are that the piezoelectric layer and mass layer can vary independently, which is not possible for the thicker piezoelectric layer, and that the mass layer increases the inertia without adding stiffness. These results suggest two additional methods to 'tune' the structure to the driving frequency and prevent charge cancellation.

Clamped Curved Plate

To further illustrate the versatility of our methodology, a series of structures with increasingly curved shapes are used as a substrate upon which a piezoelectric layer is deposited for energy harvesting. Curved devices may be required to accommodate design or configuration constraints. Alternatively, shape imperfections that occur during fabrication or service may lead to curved shapes.

The base structure for this example is the same as the previous problems with a piezoelectric layer to substrate thickness ratio of $h_p/h_s = 0.1$, but the curvature of the base structure is varied as $\kappa L/\pi = [0, 0.02, 0.04, 0.1, 0.2, 0.4, 0.6, 0.8, 1.0]$ while the surface area is constant. The structure is clamped and vibrated as before and as shown in Figure 14. The optimal distribution of piezoelectric material located on the top of the plate (the inside of the curve) is sought that maximizes the harvested power through a $1.0\,\text{k}\Omega$ resistor for an excitation frequency of 575 Hz, which is somewhere between the second and third bending modes for all curved structures. Figure 14 shows the optimized designs for a flat substrate and for two cases of curved substrates. The projections of the curved material layouts onto a flat plate for all curvatures considered are shown in Figure 15.

Figure 15 shows that the design changes with increasing base curvature. Some interesting trends are noted, such as the stark change in design with only a slight curvature added to the plate, which is due to the additional geometric stiffness and changes in mode shapes. The significant change in design as a function of base curvature implies that the optimal flat plate design is not efficient for energy harvesting on a slightly curved substrate and vice-versa. This is verified by the bar plot in Figure 16, which shows the power output for a given piezoelectric material layout for each structural curvature normalized by the power output of the optimal design for that base curvature, similar to that in Figure 9. The bar plot is diagonally dominant, meaning that each optimal design works best for the base curvature it is designed for, and reveals that the slightly curved design B will produce relatively little power on any base structure it was not designed for and vice versa. In contrast, curvatures at and above $\kappa L/\pi = 0.1$, which all have similar optimal material layouts as shown in Figure 15, produce similar amounts of power. As was the case of the flat plate in the

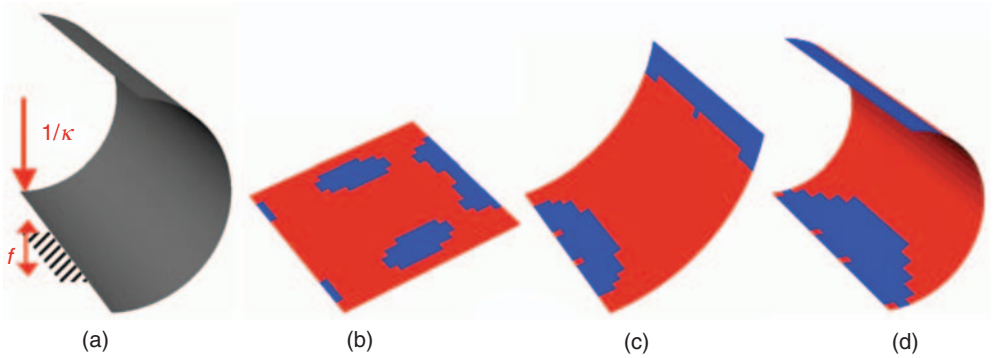

Figure 14. *(a) Problem setup and final material layouts of piezoelectric material ($h_p/h_s = 0.1$) on a curved substrate for a few different curvatures: (b) $\kappa L/\pi = 0$, (b) $\kappa L/\pi = 0.4$, (b) $\kappa L/\pi = 1.0$ (red – presence of piezoelectric material, blue – absence of piezoelectric material).*

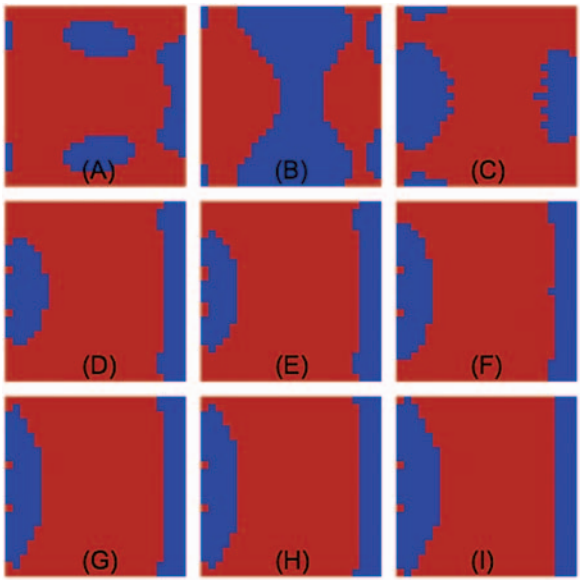

Figure 15. *Optimal material layouts for curvatures ranging from a flat plate ($\kappa L/\pi = 0$) to a half cylinder ($\kappa L/\pi = 1$). (A)–(I) Final material layouts for curvatures $\kappa L/\pi = [0, 0.02, 0.04, 0.1, 0.2, 0.4, 0.6, 0.8, 1.0]$ (red – presence of piezoelectric material, blue – its absence).*

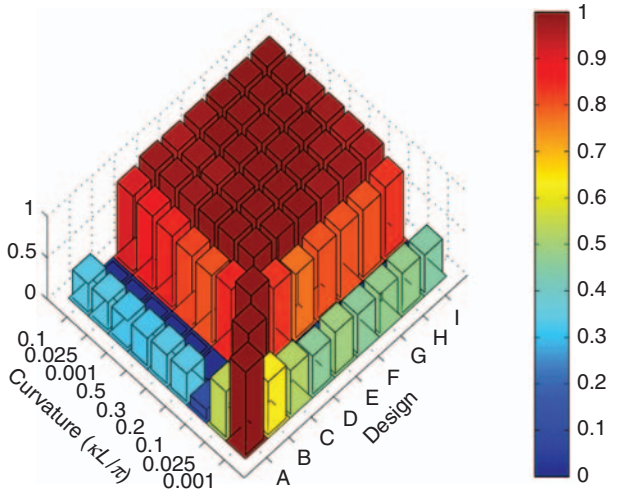

Figure 16. *Power output for a given material layout and curvature normalized to the power outputs for the optimal design of the curvature.*

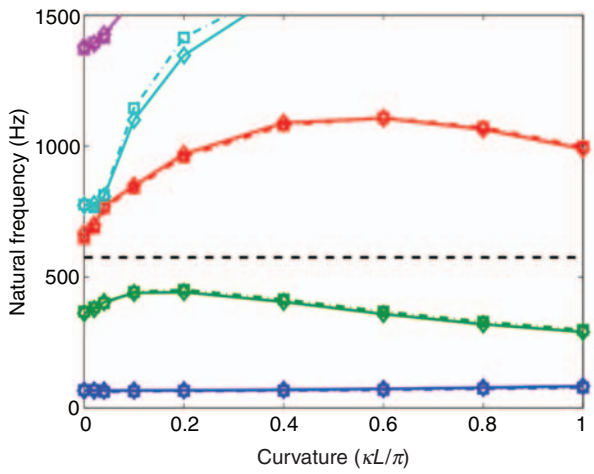

Figure 17. *Natural frequencies of bending eigenmodes for structures fully covered with piezoelectric (solid with diamonds) and those of optimized designs (dash-dot with squares). The driving frequency (dashed line – 575 Hz) is consistently between modes for all curvature values with each mode a different color for comparison.*

first example, these results are related to the locations of the natural frequencies of the structures relative to the excitation frequency. Figure 17 shows the relationship between the natural frequencies of the fully covered and optimal designs as a function of curvature. For the smaller base curvatures, large changes in natural frequency occur as a function of base curvature, while at the same time modes three and four nearly coincide. For larger base curvatures, however, the changes in natural frequency are less pronounced and the modes distinct. This correlates well with our earlier observation that differences in natural frequency and mode shape relative to the excitation frequency are significant drivers in the optimization process.

These results have general implications for manufacturing or handling of such structures due to the sensitivity in design to small shape imperfections. For example,

accidental bending or manufacturing flaws may have significant consequences in the performance of the piezoelectric harvesting system with small base curvature, but those with high base curvature would be more robust to such imperfections.

CONCLUSIONS

We presented a general methodology for the analysis and design of energy harvesting structures made from layered piezoelectric plates and their associated harvesting circuits using topology optimization. This approach provides a powerful design tool to determine the material layout of structural, piezoelectric, and electrode components, along with circuit parameters that maximize the energy harvesting performance of a piezoelectric harvesting system. Clearly defined material distributions are obtained without explicit penalization or nonlinear material interpolation schemes. Example problems demonstrated the advantages, and in many cases the necessity, of such a design approach due to either the lack of an analytical model to fully describe the structure or the large changes in response that the introduction of a piezoelectric layer may produce. In particular, we find that a design methodology solely based on finding regions of positive and negative strain is inadequate for design purposes when the piezoelectric layers significantly change the structural response. We also find that it is possible for the sensitivity of a harvester's performance to shape imperfections to change significantly as a function curvature, an important result when considering design robustness. The proposed methodology can be easily used to yield detailed designs for particular problems with application-specific objectives and constraints.

ACKNOWLEDGMENTS

We gratefully acknowledge the support of the Air Force Office of Scientific Research MURI (grant F9550-06-1-0326) 'Energy Harvesting and Storage Systems for Future Aerovehicles,' monitored by Dr B. L. Lee.

REFERENCES

Abdalla, M., Frecker, M.I., Gurdal, Z., Johnson, T. and Lindner, D.K. 2005. "Design of a Piezoelectric Actuator and Compliant Mechanism Combination for Maximum Energy Efficiency," *Smart Materials and Structures*, 14:1421–1430.

Anton, S.R. and Sodano, H.A. 2007. "A Review of Power Harvesting Using Piezoelectric Materials (2003–2006)," *Smart Materials and Structures*, 16:R1–R21.

Bathe, K. 2007. *Finite Element Procedures*, Prentice Hall, Englewood Cliffs.

Beeby, S.P., Tudor, M.J. and White, N.M. 2006. "Energy Harvesting Vibration Sources for Microsystems Applications," *Measurement Science and Technology*, 13:175–195.

Carbonari, R.C., Silva, E.C.N. and Nishiwaki, S. 2007a. "Optimum Placement of Piezoelectric Material in Piezoactuator Design," *Smart Materials and Structures*, 16:207–220.

Carbonari, R.C., Silva, E.C.N. and Paulino, G.H. 2007b. "Topology Optimization Design of Functionally Graded Bimorph-type Piezoelectric Actuators," *Smart Materials and Structures*, 16:2605–2620.

Cook-Chennault, K.A., Thambi, N. and Sastry, A.M. 2008. "Powering MEMS Portable Devices - A Review of Non-regenerative and Regenerative Power Supply Systems with Emphasis on Piezoelectric Energy Harvesting Systems," *Smart Materials and Structures*, 17(043001):1–33.

Donoso, A. and Bellido, J.C. 2009. "Systematic Design of Distributed Piezoelectric Modal Sensors/Actuators for Rectangular Plates by Optimizing the Polarization Profile," *Structural and Multidisciplinary Optimization*, 38(4):347–356.

Donoso, A. and Sigmund, O. 2009. "Optimization of Piezoelectric Bimorph Actuators with Active Damping for Static and Dynamic Loads," *Structural and Multidisciplinary Optimization*, 38(2):171–183.

Drenckhan, J., Lumsdaine, A. and Parsons, M. 2008. "Topology Optimization of a Piezoelectric Actuator on an Elastic Beam," *Journal of Intelligent Material Systems and Structures*, 19:445–455.

duToit, N.E., Wardle, B.L. and Kim, S.-G. 2005. "Design Considerations for MEMS-scale Piezoelectric Mechanical Vibration Energy Harvesters," *Integrated Ferroelectrics*, 71:121–160.

Elka, A. and Bucher, I. 2009. "Optimal Electrode Shaping for Precise Modal Electromechanical Filtering," *Structural and Multidisciplinary Optimization*, 38(6):627–641.

Elvin, N.G. and Elvin, A.A. 2009. "A General Equivalent Circuit Model for Piezoelectric Generators," *Journal of Intelligent Material Systems and Structures*, 20(1):3–9.

Erturk, A. and Inman, D.J. 2008a. "Electromechanical Modeling of Cantilvered Piezoelectric Energy Harvesters for Persistent Base Motions," In: Priya, S. and Inman, D.J. (eds), *Energy Harvesting Technologies*, Springer, US.

Erturk, A. and Inman, D.J. 2008b. "A Distributed Parameter Electromechanical Model for Cantilevered Piezoelectric Energy Harvesters," *Journal of Vibration and Acoustics*, 130(041002): 1–15.

Erturk, A. and Inman, D.J. 2008c. "On Mechanical Modeling of Cantilevered Piezoelectric Vibration Energy Harvesters," *Journal of Intelligent Material Systems and Structures*, 19(11):1311–1325.

Erturk, A. and Inman, D.J. 2008d. "Issues in Mathematical Modeling of Piezoelectric Energy Harvesters," *Smart Materials and Structures*, 17(065016):1–14.

Erturk, A. and Inman, D.J. 2009. "An Experimentally Validated Bimorph Cantilever Model for Piezoelectric Energy Harvesting From Base Excitations," *Smart Materials and Structures*, 18(025009):1–18.

Erturk, A., Tarazaga, P.A., Farmer, J.R. and Inman, D.J. 2009. "Effect of Strain Nodes and Electrode Configuration On Piezoelectric Energy Harvesting From Cantilever Beams," *Journal of Vibration and Acoustics*, 131(011010):1–11.

Felippa, C.A. 2003. "A Study of Optimal Membrane Triangles with Drilling Freedoms," *Computation Methods in Applied Mechanics and Engineering*, 192:2125–2168.

Frecker, M.I. 2003. "Recent Advances in Optimization of Smart Structures and Actuators," *Journal of Intelligent Material Systems and Structures*, 14(4–5):207–216.

Ha, Y. and Cho, S. 2006. "Design Sensitivity Analysis and Topology Optimization of Eigenvalue Problems for Piezoelectric Resonators," *Smart Materials and Structures*, 15:1513–1524.

Haug, E.J., Choi, K.K. and Komkov, V. 1986. *Design Sensitivity Analysis of Structural Systems*, Academic Press, New York.

Hemez, F. 1994. "The 3-Node Composite Shell and Isoparametric Timoshenko Beam Elements," University of Colorado, Technical Report CU-CAS-94-16, Boulder, CO.

Lefeuvre, E., Badel, A., Richard, C. and Guyomar, D. 2005a. "Piezoelectric Energy Harvesting Device Optimization by Synchronous Electric Charge Extraction," *Journal of Intelligent Material Systems and Structures*, 16(10):865–876.

Lefeuvre, E., Badel, A., Benayad, A., Lebrun, L., Richard, C. and Guyomar, D. 2005b. "A Comparison Between Several Approaches of Piezoelectric Energy Harvesting," *Journal de Physique IV France*, 128:177–186.

Lefeuvre, E., Badel, A., Richard, C. and Guyomar, D. 2007. "Energy Harvesting Using Piezoelectric Materials: Case of Random Vibrations," *Journal of Electroceramics*, 19:349–355.

Lesieutre, G.A., Ottman, G.K. and Hofmann, H.F. 2004. "Damping as a Result of Piezoelectric Energy Harvesting," *Journal of Sound and Vibration*, 269(3–5):991–1001.

Kang, Z. and Tong, L. 2008a. "Integrated Optimization of Material Layout and Control Voltage for Piezoelectric Laminated Plates," *Journal of Intelligent Material Systems and Structures*, 19(8):889–904.

Kang, Z. and Tong, L. 2008b. "Topology Optimization-based Distribution Design of Actuation Voltage in Static Shape Control of Plates," *Computers and Structures*, 86:1885–1893.

Kim, S., Clark, W.W. and Wang, Q.-M. 2005a. "Piezoelectric Energy Harvesting with a Clamped Circular Plate: Analysis," *Journal of Intelligent Material Systems and Structures*, 16(10):847–854.

Kim, S., Clark, W.W. and Wang, Q.-M. 2005b. "Piezoelectric Energy Harvesting with a Clamped Circular Plate: Experimental Study," *Journal of Intelligent Material Systems and Structures*, 16(10): 855–863.

Marinkovic, D., Koppe, H. and Gabbert, U. 2007. "Accurate Modeling of the Electric Field Within Piezoelectric Layers for Active Composite Structures," *Journal of Intelligent Material Systems and Structures*, 18:503–513.

Militello, C. and Felippa, C.A. 1991. "The First ANDES Elements: 9-Dof Plate Bending Triangles," *Computation Methods in Applied Mechanics and Engineering*, 93:217–246.

Ottman, G.K., Hofmann, H.F., Bhatt, A.C. and Lesieutre, G.A. 2002. "Adaptive Piezoelectric Energy Harvesting Circuit for Wireless Remote Power Supply," *IEEE Transactions on Power Electronics*, 17(5):669–676.

Ottman, G.K., Hofmann, H.F. and Lesieutre, G.A. 2003. "Optimized Piezoelectric Energy Harvesting Circuit Using Step-down Converter in Discontinuous Conduction Mode," *IEEE Transactions on Power Electronics*, 18(2):696–703.

Priya, S. 2007. "Advances in Energy Harvesting Using Low Profile Piezoelectric Transducers," *Journal of Electroceramics*, 19:167–184.

Renno, J.M., Daqaq, M.F. and Inman, D.J. 2009. "On the Optimal Energy Harvesting from a Vibration Source," *Journal of Sound and Vibration*, 320(1–2):386–405.

Schittkowski, K. 1985. "NLPQL: A FORTRAN Subroutine Solving Constrained Nonlinear Programming Problems," *Annals of Operations Research*, 5:485–500.

Shu, Y.C. and Lien, I.C. 2006a. "Efficiency of Energy Conversion for a Piezoelectric Power Harvesting System," *Journal of Micromechanics and Microengineering*, 16:2429–2438.

Shu, Y.C. and Lien, I.C. 2006b. "Analysis of Power Output for Piezoelectric Energy Harvesting Systems," *Smart Materials and Structures*, 15:1499–1512.

Shu, Y.C., Lien, I.C. and Wu, W.J. 2007. "An Improved Analysis of The SSHI Interface in Piezoelectric Energy Harvesting," *Smart Materials and Structures*, 16:2253–2264.

Sodano, H.A. and Inman, D.J. 2004. "A Review of Power Harvesting from Vibration using Piezoelectric Materials," *The Shock and Vibration Digest*, 36:197–205.

Williams, C.B. and Yates, R.B. 1996. "Analysis of a Micro-electric Generator for Microsystems," *Sensors and Actuators*, 52:8–11.

Zheng, B., Chang, C.-J. and Gea, H.C. 2009. "Topology Optimization of Energy Harvesting Devices using Piezoelectric Materials," *Structural and Multidisciplinary Optimization*, 38(1):17–23.